LiAISON-Supplemented Navigation for Geosynchronous and Lunar L_1 Orbiters

Jason M. Leonard*, Ryan M. McGranaghan*,
Kohei Fujimoto*, George H. Born†,
Jeffrey S. Parker‡, and Rodney L. Anderson§

A high-fidelity simulation is developed to test the theory that relative range and range-rate measurements between a satellite in a geosynchronous orbit and a satellite in orbit about the Earth-Moon L_1 point may be used to improve the navigation accuracy of both satellites, compared with ground-only tracking. Recent research has determined that satellite-to-satellite range measurements between these two orbits are sufficient to perform absolute state estimation as well as relative state estimation of both satellites – a technology known as LiAISON (Linked Autonomous Interplanetary Satellite Orbit Navigation). This study quantifies the improvement in accuracy when LiAISON is used to supplement ground tracking of one or both satellites in a very realistic simulation. Orbit determination techniques show that the inclusion of LiAISON measurements with ground tracking observations can greatly improve absolute position and velocity estimates for both satellites in geosynchronous orbit and about the Earth-Moon L_1 point.

I. Introduction

Through the use of satellite-to-satellite tracking (SST), new navigation techniques have revealed the ability to perform accurate absolute navigation of one or more satellites in a given constellation. Satellite navigation for low Earth orbit (LEO) has been revolutionized through the Global Positioning System (GPS) and the use of accurate atomic clocks for time keeping. Some of the successful aspects of GPS have been extended to a relatively new navigation technique known as LiAISON (Linked Autonomous Interplanetary Satellite Orbit Navigation).[1,2] LiAISON has the ability to extend some aspects of GPS to orbits in new regimes beyond LEO for which a minimum of two satellites in a LiAISON constellation are all that is necessary to perform absolute autonomous navigation.

LiAISON navigation typically involves two or more satellites collecting relative tracking data to determine the absolute positions and velocities of each vehicle in space over time. In most applications, relative measurements only permit a system of vehicles to determine their relative states. For instance, any normal constellation of Earth orbiters could rotate the entire constellation about the Earth and achieve the same relative tracking measurements. LiAISON navigation works because the spacecraft constellation is in an asymmetric gravity field: one that involves both the Earth and the Moon. A time-series of satellite-to-satellite measurements in such a system is unique and fixed to the positions of the Earth and Moon. Therefore, LiAISON navigation results in the determination of both satellites' absolute trajectories using relative measurements.

The LiAISON navigation technique has been shown to be very beneficial when applied to the navigation of lunar satellites, including low lunar orbiters and lunar libration orbiters.[1–8] This technique has been shown to generate better navigation accuracy than typical ground-only tracking. It has been recently hypothesized

*Research Assistant, University of Colorado, Boulder, CO 80309. AIAA Student Member.
†Director of the Colorado Center for Astrodynamics Research, University of Colorado, Boulder, CO 80309. AIAA Fellow.
‡Member of Technical Staff, Jet Propulsion Laboratory, California Institute of Technology, M/S 301-121, 4800 Oak Grove Dr., Pasadena, CA 91109. Currently an Assistant Research Professor at the University of Colorado, Boulder, CO 80309. AIAA Senior Member.
§Member of Technical Staff, Jet Propulsion Laboratory, California Institute of Technology, M/S 301-121, 4800 Oak Grove Dr., Pasadena, CA 91109. AIAA Member.

that the benefits of LiAISON may apply to Earth orbiting satellites as well. This study has elected to analyze the benefits of LiAISON applied to geosynchronous Earth orbiters because those satellites have a high demand for improved navigation accuracy. The navigation of geosynchronous Earth orbit (GEO) satellites is challenging because their positions do not change rapidly over time relative to their ground tracking stations. GEO navigators rely on complex measurements such as optical tracking in order to achieve position accuracies as low as 10 meters.[9]

A dedicated navigation satellite anywhere near the Moon has a huge advantage over ground stations when it comes to tracking GEO satellites using radiometric data. Where the range between a GEO satellite and a ground station is typically very constant, the range between a GEO satellite and a satellite near the Moon is very dynamic. Further, the uniqueness of a halo orbit about the Earth-Moon L_1 point generates a clear, dynamic signature in the relative SST observations. Clear signals in the data can be used to lock onto the position and velocity of both satellites.

This paper examines a new navigation concept in detail, studying the benefits of supplementing standard ground tracking measurements of two satellites in the Earth-Moon system with relative satellite-to-satellite tracking observations made between these satellites. A concurrent study has demonstrated the viability of the LiAISON technique applied to a constellation of two satellites, where one is in orbit about the lunar L_1 point and the other is at GEO.[10,11] This paper quantifies the improvement in accuracy that one may expect by supplementing conventional radiometric ground tracking with LiAISON measurements.

This study develops high-fidelity simulations to quantify the benefits of LiAISON applied to tracking GEO and L_1 satellites. The scenario begins with typical ground-only tracking to establish a baseline navigation accuracy of both satellites. This ground-only tracking involves radiometric data to remain consistent throughout the study. LiAISON measurements are then introduced to quickly improve the navigation accuracy of both satellites. The simulations include dynamical modeling errors, measurement errors, and measurement biases. Furthermore, the measurements include large measurement gaps to simulate other activities being performed by each asset. A tracking schedule analysis is performed over a wide range of possible observation pass gaps. The results are compared to both continuous ground-only tracking and LiAISON tracking.

II. LiAISON Navigation

Autonomous SST relies on an ability to estimate the absolute positions of a spacecraft without the use of ground station observations. To do so, the size, shape, and orientation of the satellite's orbit must be observable from the measurements available between the linked spacecraft. The observability of the system depends on one of these satellites occupying a unique trajectory. The determining factor in whether a unique trajectory can exist, and thus whether LiAISON is possible, is the acceleration function acting on the orbiter. No unique orbits exist in a symmetric acceleration field, one in which the function and its time derivative are symmetric. Even in regions with desired asymmetric perturbations, uncertainties in the force model and observation noise can counteract these effects in the accelerations and prevent SST orbit determination. As a result, the asymmetric acceleration effects must be great enough to outweigh the uncertainties and force model issues that arise.

Acceleration functions with sufficient asymmetry for LiAISON are provided by three-body systems that give rise to libration point orbits (LPOs). The third-body perturbation of the Moon is sufficient to provide the asymmetry necessary for locally unique trajectories to exist. Due to the effects of the gravitational forces of the Moon and Earth, lunar LPOs can only have one orientation with respect to this system. L_1 and L_2 LPOs are specifically well suited for LiAISON because they are locally unique and reside in regions where the asymmetry of the accelerations is strong. Under these conditions a spacecraft at one of these Lagrange points can uniquely and absolutely determine the state of a second satellite using crosslink range measurements without ground-based observations.

Several papers have demonstrated the benefits of LiAISON navigation applied to satellite constellations at the Moon. This effort has been motivated by NASA's aim to develop a permanent presence at the Moon. Hill et al. explored the cases of 2–4 satellites placed in combinations of low lunar orbits and libration orbits about the Earth-Moon L_1 and/or L_2 points.[1,3,5,6] A potential mission was examined in detail, including only two satellites: one in a 100-km polar orbit about the Moon and the other in a libration orbit about the Earth-Moon L_2 point.[3] The results demonstrated that satellites may be navigated at the Moon using realistic constraints and achieve accuracies on the order of 100 meters or less for halo orbiters and 10 meters

or less for low lunar orbiters. Any ground tracking passes would only improve the solutions.

The scenario examined in this paper extends the concepts of LiAISON navigation beyond constellations fixed at the Moon. This study considers placing one satellite in a geosynchronous orbit, since there is significant interest in improving the navigation of GEO satellites; future studies will examine other orbits, including low Earth orbits, lunar transfers, and interplanetary trajectories. It may be the case that NASA's lunar development warrants a dedicated navigation satellite; this study demonstrates that such a satellite may be able to offer substantial benefits to Earth-orbiting satellites as well.

In order to make an accurate analysis of a LiAISON navigation solution between an L_1 and GEO constellation, an understanding of current navigation accuracies for both regimes is necessary. For the GEO regime, most commercial operators track GEO satellites to within a kilometer in position. More stringent requirements are necessary for the TDRSS system. A position navigation accuracy of less than 100 meters is required, though in practice position navigation solutions tend to be accurate to within 30 meters.[12] Sabol has shown that range-only observations can be used to perform orbit determination to within 30 meters in position for GEO satellites by using several different tracking stations.[13] Moreau et al. have shown that one could track GPS signals from GEO for a position accuracy of about 15 meters.[14] Tombasco showed that optical tracking could reduce the uncertainty of a GEO orbit to within 10 meters.[9]

Navigation of satellites in Lunar LPOs has only recently been done through the ARTEMIS mission in late 2010 through 2011.[15,16] The primary measurement type for this mission was radiometric tracking data from the Deep Space Network (DSN), the Universal Space Network (USN), and the Berkeley Ground Station (BGS).[17,18] The DSN navigation data used for the ARTEMIS mission was range and Doppler measurements with a tracking pass schedule of 3.5 hours of data every other day making an attempt to alternate stations from the northern and southern hemispheres. Navigation solutions were obtained for each satellite on the order of 100 meters in position and approximately 1 mm/s in velocity.

The effectiveness of LiAISON is evaluated using orbit determination solely composed of range and range-rate measurements between two participating spacecraft. A dedicated navigation satellite anywhere near the Moon has an advantage over ground stations for tracking GEO satellites using radiometric data. While most satellites are only visible from ground stations at certain times, including those orbiting around the L_1 point, a link between a GEO and L_1 satellite has nearly continuous visibility. Figure 1 demonstrates the near continuous dynamic range measurements between an example GEO satellite and a satellite traversing an LPO about the Earth-Moon L_1 point versus the range of a GEO orbit tracked by a ground station. One can see clear signals in the data that may be used to lock onto the position and velocity of both satellites.

To demonstrate the advantages and capabilities of a LiAISON architecture, a simulation involving two satellites, one in a lunar L_1 LPO and the other at GEO, is examined. Observations with realistic errors and uncertainties were generated for the satellite constellation. The satellite orbits were determined using a high fidelity integration and gravity modeling. A conventional Kalman filter was used to process the observations.

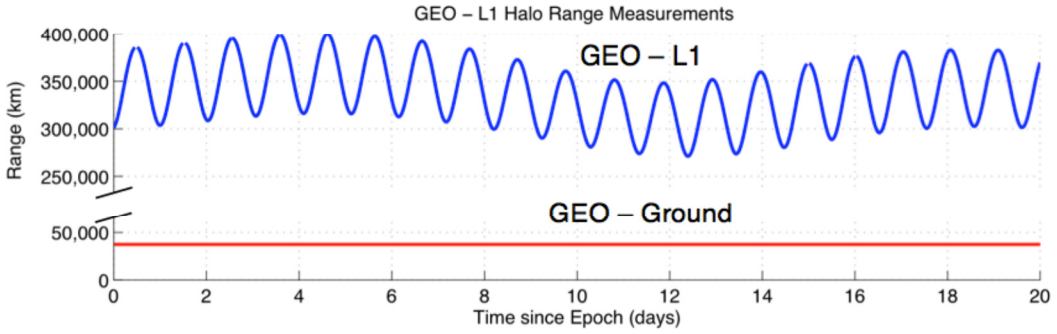

Figure 1. Satellite constellation geometry for truth model simulations for LiAISON and ground tracking.

III. Dynamical Model and Linearization

Modern orbit determination algorithms commonly employ a propagation of the state and uncertainty along a reference trajectory followed by measurement processing in order to obtain a more accurate estimate of the satellites state. A majority of the orbit determination methods use a linearization of the states in order to propagate state deviations and their uncertainties over time along a specified reference trajectory. In this section, the theory of the associated dynamical equations for the reference trajectory are derived and then linearized for use in a conventional Kalman filter that has been derived in Section V.

A. Satellite State Dynamics

In this work, an attempt is made at estimating the state of two satellites, their solar radiation pressure (SRP) coefficients, and associated biases in the measurement equations. A simplified state vector is used that contains both satellites' positions and velocities as well as the constant terms previously mentioned as given in Eq. 1. The range bias term $\boldsymbol{\rho}_{\text{bias}}$ does not affect the satellite state dynamics but is part of the estimated state and is used in the filter and measurement equations.

$$\mathbf{X} = \begin{bmatrix} \mathbf{r}_1^{\mathrm{T}} & \mathbf{v}_1^{\mathrm{T}} & \mathbf{r}_2^{\mathrm{T}} & \mathbf{v}_2^{\mathrm{T}} & \delta C_{R,1} & \delta C_{R,2} & \mathbf{w}_1^{\mathrm{T}} & \mathbf{w}_2^{\mathrm{T}} & \boldsymbol{\rho}_{\text{bias}}^{\mathrm{T}} \end{bmatrix}^{\mathrm{T}}. \tag{1}$$

The first four elements of the state vector are the position and velocities (both vectors have a dimension of 3) of the two spacecraft in the Geocentric Celestial Reference Frame (GCRF). The remaining elements of the state vector are deviations from *a priori* values of the SRP reflectivity coefficients, empirical acceleration vectors for both satellites (each vector has a dimension of 3), and the range biases being estimated for each observation link (a total of 5 in this work).

The time evolution of the state vector $\mathbf{X}$ is given by a system of nonlinear first order differential equations. In this work, the time evolutions of the position and velocity vectors of a spacecraft are given the following dynamics:

$$\begin{bmatrix} \dot{\mathbf{r}}_i \\ \dot{\mathbf{v}}_i \end{bmatrix} = \begin{bmatrix} \mathbf{v}_i \\ \mathbf{a}_g(t, \mathbf{r}_i) + \mathbf{a}_{SRP}(t, \mathbf{r}_i) + \mathbf{a}_{n\text{-}body}(\mathbf{r}_i, \mathbf{r}_{\oplus 3}) + [\gamma]_{RTN}^{\mathrm{T}} \mathbf{w}_i \end{bmatrix}, \tag{2}$$

where $\mathbf{a}_g(t, \mathbf{r})$ is the gravitational accelerations due to two-body and Earth's non-spherical body. In addition to the gravitational acceleration, SRP $\mathbf{a}_{SRP}(t, \mathbf{r}_i)$, n-body perturbations $\mathbf{a}_{n\text{-}body}(\mathbf{r}_i, \mathbf{r}_{\oplus 3})$, and empirical accelerations $\mathbf{w}_i$, are acting upon the spacecraft. The Earth's gravitational potential including the two-body term is commonly given in terms of spherical harmonics as

$$U(x, y, z) = \frac{\mu}{r}\left[1 + \sum_{l=2}^{\infty}\sum_{m=0}^{l}\left(\frac{R}{r}\right)^{l} P_{l,m}(\sin\phi_{\text{gc}})\left\{C_{l,m}\cos(m\lambda) + S_{l,m}\sin(m\lambda)\right\}\right]. \tag{3}$$

The normalized Cartesian spherical harmonic model is used in this work for the calculation of local gravitational acceleration.[19] The normalized Cartesian model does not rely on spherical coordinates and does not contain any singularities as seen in the classical formulation. The acceleration vector from spherical harmonics is given in International Terrestrial Reference Frame (ITRF) and must be rotated back to GCRF. The conversion from the Earth-centered, Earth-fixed reference frame to the Earth-centered inertial reference frame is computed through the 1976 IAU Precession, 1980 IAU Nutation (no IERS corrections are used), Earth rotation parameters, and polar motion.[20]

The solar radiation pressure model used is based on a constant area, constant reflectance model. The shadow model used determines an approximate value of the percentage of the Sun's face that is visible from the spacecraft location. The radii of the bodies used in the shadow model are taken from the JPL DE405 (Ref 21 and 22) ephemeris, and the solar radiation pressure is adjusted based on the distance from the sun. The acceleration due to SRP is given by

$$\mathbf{a}_{SRP} = P_{SRP} C_R \frac{A_\odot}{m} \frac{\mathbf{r}_{\odot sat}}{|\mathbf{r}_{\odot sat}|}, \tag{4}$$

where C_R is the reflectivity of the spacecraft, $A_\odot$ is the cross-sectional area of the spacecraft facing the Sun, m is the mass of the spacecraft, $\mathbf{r}_{\odot sat}$ is the vector from the center of the Sun to the spacecraft, and P_{SRP} is the solar radiation pressure of the Sun. The value used for P_{SRP} is about 4.5298×10^{-6} Pa at one AU. The variation in P_{SRP} for various distances from the sun is calculated by

$$P_{SRP} = P_{SRP,AU} \frac{(149,597,870\ km)^2}{|\mathbf{r}_{\odot sat}|^2}. \tag{5}$$

In addition to the central body non-spherical gravitational acceleration, the gravitation effects of multiple bodies (n-body) are determined. This can include extra perturbations due to the Sun, Moon, or other planets in the solar system. The acceleration $\mathbf{a}_{n\text{-}body,i}$ due to the gravitational attraction of body k of the n-bodies is given by

$$\mathbf{a}_{n\text{-}body,k} = -\mu_k \left[\frac{\mathbf{r}_{k,sat}}{r_{k,sat}^3} + \frac{\mathbf{r}_{\oplus,k}}{r_{\oplus,k}^3} \right], \tag{6}$$

where μ_k is the gravitational parameter of the k^{th} body, $\mathbf{r}_{k,sat}$ is the vector from the k^{th} body to the satellite, and $\mathbf{r}_{\oplus,k}$ is the vector from the central body to the k^{th} body. The position of celestial bodies is computed from the JPL DE 405 ephemerides.[21,22]

The local empirical acceleration disturbances experienced by each of the satellites are modeled as first-order Gauss-Markov processes. The process is governed by the following equations of motion

$$\dot{\mathbf{w}}_i = -\boldsymbol{\beta}_i \mathbf{w}_i + \mathbf{u}_i(t), \tag{7}$$

where $\mathbf{w}_i$ is the local empirical acceleration vector, $\boldsymbol{\beta}$ is a vector of correlation time constants, and $\mathbf{u}(t)$ is white noise with $\mathrm{E}[\mathbf{u}(t)] = 0$ and $\mathrm{E}\left[\mathbf{u}(t)\mathbf{u}^{\mathrm{T}}(\tau)\right] = \sigma^2\delta(t-\tau)$. The acceleration disturbances, $\mathbf{w}_i$ are given in a local coordinate frame that coincides with the SRP direction. The rotation matrix $[\gamma]_{RTN}$ defines the rotation from the local radial, transverse, and normal (RTN) frame to the GCRF frame. The RTN frame transformation is given by

$$\begin{aligned} \mathbf{u}_R &= \frac{\mathbf{r}_{\odot sat}}{|\mathbf{r}_{\odot sat}|} \\ \mathbf{u}_T &= \mathbf{u}_N \times \mathbf{u}_R \\ \mathbf{u}_N &= \frac{\mathbf{u}_R \times [0,0,1]^{\mathrm{T}}}{|\mathbf{u}_R \times [0,0,1]^{\mathrm{T}}|} \end{aligned} \tag{8}$$

where $\mathbf{u}_R$, $\mathbf{u}_T$, and $\mathbf{u}_N$ are unit vectors in the RTN frame. The transformation matrix relating the RTN and GCRF frame is thus $[\gamma]_{RTN} = [\mathbf{u}_R, \mathbf{u}_T, \mathbf{u}_N]^{\mathrm{T}}$. The local acceleration disturbances in the RTN frame can now be translated into the GCRF frame.

The remaining terms in the state vector $\mathbf{X}$ are considered to be constants. The continuous-time dynamics of these constants thus take the form

$$\delta\dot{C}_{R,1} = 0, \tag{9}$$

$$\delta\dot{C}_{R,2} = 0, \tag{10}$$

and

$$\dot{\boldsymbol{\rho}}_{\text{bias}} = \mathbf{0}. \tag{11}$$

The state dynamics given in equations above can be assembled and written in the convenient continuous-time model of the form

$$\dot{\mathbf{X}}(t) = \boldsymbol{f}(t, \mathbf{X}(t), \mathbf{u}(t)), \tag{12}$$

where $\mathbf{u}(t)$ is a zero-mean Gaussian white process noise vector. This continuous-time dynamical equation is a first order ordinary differential equation that can be solved using a variety of integration methods.

B. Linearized State Dynamics

The orbit determination filter used in this work requires linearization of the dynamics and measurement models about an estimate. A conventional Kalman filter is used in which the trajectory is linearized about the most current best estimate. This filter requires the partial derivatives of the state with respect to an initial state from t_k to t_{k+1}. The necessary linearization parameters are the state transition matrix

$$\boldsymbol{\Phi}(t_{k+1}, t_k) = \frac{\partial \mathbf{X}(t_{k+1})}{\partial \mathbf{X}(t_k)}, \tag{13}$$

and the process noise transition matrix

$$\boldsymbol{\Gamma}(t_{k+1}, t_k) = \frac{\partial \mathbf{X}(t_{k+1})}{\partial \mathbf{u}(t_k)}. \tag{14}$$

The state transition matrix is obtained by integrating

$$\dot{\Phi}(t, t_k) = A(t)\Phi(t, t_k) \tag{15}$$

subject to the initial conditions $\Phi(t_k, t_k) = I$ along with the reference trajectory $\mathbf{X}^*(t)$. The matrix $A(t)$ is evaluated along the reference trajectory $\mathbf{X}^*(t)$ and is given by

$$A(t) = \frac{\partial F(\boldsymbol{X}^*, t)}{\partial \boldsymbol{X}}, \tag{16}$$

where $F(\mathbf{X}^*, t)$ is the time derivative of the state vector $\mathbf{X}(t)$. These Jacobian matrices can then be used to linearize the dynamics as seen in Eq. 17.

$$\left[\mathbf{X}_{k+1} - \bar{\mathbf{X}}_{k+1}\right] = \boldsymbol{\Phi}(t_{k+1}, t_k)\left[\mathbf{X}_k - \hat{\mathbf{X}}_k\right] + \boldsymbol{\Gamma}(t_{k+1}, t_k)\mathbf{u}_k, \tag{17}$$

where $\hat{\mathbf{X}}_k$ is the *a posteriori* state estimate at the sample time t_k and $\bar{\mathbf{X}}_{k+1}$ is the *a priori* state estimate at the sample time t_{k+1}.

IV. Measurement Model and Linearization

Measurement processing is necessary in order for the Kalman filter to update the state and uncertainty estimate. The Kalman filter used in this analysis requires a measurement model and its linearized form. This section introduces the theory behind the nonlinear measurement model used in this study along with the linearization of the measurement model along its reference trajectory.

A. Measurement Model

A simplified measurement model is used for this research. The filter in this work uses an idealized range and range-rate measurement between the two satellites. A complex model that solves for time of flight and clock errors is not necessary for the determination if the proposed navigation solution is feasible. Thus, we use the idealized range and range-rate equations to determine if the navigation solution is at all possible. An idealized range between two satellites is given as

$$\rho = \sqrt{(\mathbf{r}_1 - \mathbf{r}_2) \cdot (\mathbf{r}_1 - \mathbf{r}_2)} + \rho_{bias} + \rho_{noise}, \tag{18}$$

where $\mathbf{r}_1$ and $\mathbf{r}_2$ are the position vectors of the two satellites. The terms ρ_{bias} and ρ_{noise} are error terms in the idealized range equation. The idealized range-rate between two satellites is thus

$$\dot{\rho} = \frac{\boldsymbol{\rho} \cdot \dot{\boldsymbol{\rho}}}{\rho} + \dot{\rho}_{noise}, \tag{19}$$

where $\boldsymbol{\rho} = \mathbf{r}_1 - \mathbf{r}_2$ is the position vector of one satellite with respect to the other and $\dot{\boldsymbol{\rho}} = \dot{\mathbf{r}}_1 - \dot{\mathbf{r}}_2$ is the relative velocity between the two satellites. The error term in the idealized range-rate equation is thus given as $\dot{\rho}_{noise}$.

Similarly to the satellite-to-satellite idealized range and range-rate equations, a set of equations for ground based tracking can be derived. For this set of equations, the position and velocity vectors of the second satellite, $\mathbf{r}_2$ and $\dot{\mathbf{r}}_2$, can be replaced by the position and velocity vectors, $\mathbf{r}_s$ and $\dot{\mathbf{r}}_s$, of a ground station in GCRF coordinates. In this work, the three main DSN stations are chosen: Goldstone, Madrid, and Canberra. These stations track the Lunar L_1 orbiter. Another ground station, located in California, tracks the GEO satellite. An elevation mask of 10 degrees is used for each tracking station.

B. Linearized Measurement Equations

Similar to the dynamical model, the filter used in this study requires a linearized observation model. The filter requires the partial derivatives of the measurement model with respect to the state that is linearized about the most current state estimate. The measurement equation for this system can be written in the form

$$\boldsymbol{Y} = \boldsymbol{h}(\mathbf{X}, \mathbf{u}) + \boldsymbol{\nu}. \tag{20}$$

The nonlinear observation equation $\boldsymbol{h}(\mathbf{X}, \mathbf{u})$ is a function of the range and range-rate equations previously defined. The observation function can be rewritten as

$$\boldsymbol{h}(\mathbf{X}, \mathbf{u}) = \begin{bmatrix} \rho_{LiAISON} & \dot{\rho}_{LiAISON} & \boldsymbol{\rho}_{ground}^{\mathrm{T}} & \dot{\boldsymbol{\rho}}_{ground}^{\mathrm{T}} \end{bmatrix}^{\mathrm{T}}. \tag{21}$$

The Jacobians required for the filter are thus

$$\tilde{H}_{\mathbf{X},k} = \frac{\partial \boldsymbol{h}}{\partial \mathbf{X}_k} \quad \text{and} \quad \tilde{H}_{\mathbf{u},k} = \frac{\partial \boldsymbol{h}}{\partial \mathbf{u}_k}. \tag{22}$$

Since the linearized measurement equations are not dependent on the process noise $\mathbf{u}_k$, the Jacobian $\tilde{H}_{\mathbf{u},k} = \mathbf{0}$. The Jacobian with respect to the state however is nonzero and must be calculated either analytically or numerically. In this work, an analytical partial derivative is simple and can be computed. The partial derivatives with respect to the satellite's position and velocity as well as the ground stations position and velocity are not given here but are easily computed. The partial derivative of the bias and noise terms are given as

$$\frac{\partial \boldsymbol{h}}{\partial \rho_{bias}} = 1 \quad \text{and} \quad \frac{\partial \boldsymbol{h}}{\partial \rho_{noise}} = 0. \tag{23}$$

This completes the necessary definitions of the linearized measurement equations.

V. Kalman Filter

In this work, a conventional Kalman filter (CKF) is used to estimate the state of the satellites and the constant parameters given in Eq. 1. The CKF is a sequential processing algorithm and allows one to mimic real time observation processing as more measurements are received. The algorithm used is derived from Ref. 23. If $\mathbf{X}^*(t)$ is a reference trajectory that is near the truth trajectory in the linear regime, then one can define a state deviation vector $\mathbf{x}(t)$ as

$$\mathbf{x}(t) = \mathbf{X}(t) - \mathbf{X}^*(t). \tag{24}$$

An estimate of the state deviation, $\hat{x}_k$, for a sequential Kalman filter and the associated covariance matrix, P_k, can be propagated forward in time t_k by

$$\bar{x}_{k+1} = \Phi(t_{k+1}, t_k)\hat{x}_k, \tag{25}$$

$$\bar{P}_{k+1} = \Phi(t_{k+1}, t_k) P_k \Phi(t_{k+1}, t_k)^{\mathrm{T}} + \bar{Q}(t), \tag{26}$$

$$\bar{Q}(t) = \Gamma(t_{k+1}, t_k) Q \Gamma(t_{k+1}, t_k)^{\mathrm{T}}, \tag{27}$$

where $\bar{x}_{k+1}$ and $\bar{P}_{k+1}$ are the *a priori* estimates of the state deviation and covariance matrix, $\bar{Q}(t)$ is the process noise covariance matrix, and the linearized state dynamics were previously given. Eq. 27 can be calculated and is well known in controls and orbit determination literature.[23] However, in this study the *a priori* process noise covariance matrix needs to be rotated from the RTN frame to the GCRF frame. Since the equations that define the matrix $\bar{Q}(t)$ defined in Ref. 23 are given in a specific frame. Here, that frame is defined as being the RTN frame and thus a rotation of the process noise covariance matrix from the local RTN frame to the GCRF frame is necessary. This is accomplished by the following rotations of the RTN process noise covariance matrix:

$$\bar{Q}_{GCRF} = \begin{bmatrix} [\gamma]_{RTN}^{\mathrm{T}} \bar{Q}_{(\mathbf{r},\mathbf{r})} [\gamma]_{RTN} & [\gamma]_{RTN}^{\mathrm{T}} \bar{Q}_{(\mathbf{r},\mathbf{v})} [\gamma]_{RTN} & [\gamma]_{RTN}^{\mathrm{T}} \bar{Q}_{(\mathbf{r},\mathbf{a})} \\ [\gamma]_{RTN}^{\mathrm{T}} \bar{Q}_{(\mathbf{v},\mathbf{r})} [\gamma]_{RTN} & [\gamma]_{RTN}^{\mathrm{T}} \bar{Q}_{(\mathbf{v},\mathbf{v})} [\gamma]_{RTN} & [\gamma]_{RTN}^{\mathrm{T}} \bar{Q}_{(\mathbf{v},\mathbf{a})} \\ \bar{Q}_{(\mathbf{a},\mathbf{r})} [\gamma]_{RTN} & \bar{Q}_{(\mathbf{a},\mathbf{v})} [\gamma]_{RTN} & \bar{Q}_{(\mathbf{a},\mathbf{a})} \end{bmatrix}, \tag{28}$$

where the subscripts $\mathbf{r}$, $\mathbf{v}$, and $\mathbf{a}$ denote the position, velocity, and acceleration respectively for the local RTN process noise covariance matrix. Each of the submatricies, $\bar{Q}_{(\cdot,\cdot)}$, has a dimension of 3×3 in the RTN coordinate frame. With this information, the *a priori* state deviation and covariance matrix can be calculated.

Assuming that an observation $\mathbf{Y}_{k+1}$ exists at time t_{k+1}, the linearized observation equation is given by

$$\mathbf{y}_{k+1} = \tilde{H}_{k+1} \mathbf{x}_{k+1} + \boldsymbol{\epsilon}_{k+1}, \tag{29}$$

where $\mathbf{y}_{k+1}$ is the observation deviations from the compute observations along the reference trajectory $\mathbf{y}_{k+1} = \mathbf{Y}_{k+1} - \mathbf{Y}(\mathbf{X}^*_{k\,|\,1}, t)$, $\boldsymbol{\epsilon}_{k+1}$ is the observation noise, and $\tilde{H}_{k+1}$ is the linearized measurement equations previously defined. The observation noise, $\boldsymbol{\epsilon}_{k+1}$, is assumed to have the following statistics:

$$\mathrm{E}[\boldsymbol{\epsilon}_{k+1}] = 0, \tag{30}$$

and

$$\mathrm{E}[\boldsymbol{\epsilon}_{k+1} \boldsymbol{\epsilon}_{k+1}^{\mathrm{T}}] = R_{k+1}. \tag{31}$$

The best estimate of the state deviation, $\mathbf{x}_{k+1}$, can be obtained by

$$\hat{\mathbf{x}}_{k+1} = \bar{\mathbf{x}}_{k+1} + K_{k+1}[\mathbf{y}_{k+1} - \tilde{H}_{k+1} \bar{\mathbf{x}}_{k+1}], \tag{32}$$

where the Kalman gain, K_{k+1}, is defined by

$$K_{k+1} = \bar{P}_{k+1} \tilde{H}_{k+1}^T \left[\tilde{H}_{k+1} \bar{P}_{k+1} \tilde{H}_{k+1}^T + R_{k+1} \right]^{-1}. \tag{33}$$

The *a posteriori* state estimate, $\hat{\mathbf{X}}(t)$, can then be obtained by

$$\hat{\mathbf{X}}_{k+1} = \mathbf{X}^*_{k+1} + \hat{\mathbf{x}}_{k+1}. \tag{34}$$

The *a posteriori* covariance matrix can then be computed. In order to prevent P_{k+1} from losing its symmetric condition, the Joseph formulation is used and is given by

$$P_{k+1} = (I - K_{k+1} \tilde{H}_{k+1}) \bar{P}_{k+1} (I - K_{k+1} \tilde{H}_{k+1})^T + K_{k+1} R_{k+1} K_{k+1}^T. \tag{35}$$

This formulation of P_{k+1} will always yield a symmetric matrix but it may lose its positive definite condition for poorly observed systems.

VI. LiAISON Truth Model Simulations

A truth model simulation of the LiAISON configuration is necessary in order to determine the effectiveness of the proposed filter. In the truth model, a time history of the two satellites states are obtained through numerical integration of the equations of motion previously defined. The simulation then generates SST observations between the two satellites and a fictitious DSN network. The DSN network consists of radiometric tracking from Goldstone, California, Madrid, Spain, and Canberra, Australia. A single ground station tracking the GEO satellite is located in Sky Valley, California. Once the truth simulation is generated with the observations, the filter analysis can be performed. Figure 2 shows the LiAISON scenario configuration for this study and the tracking links between the two satellites and the ground.

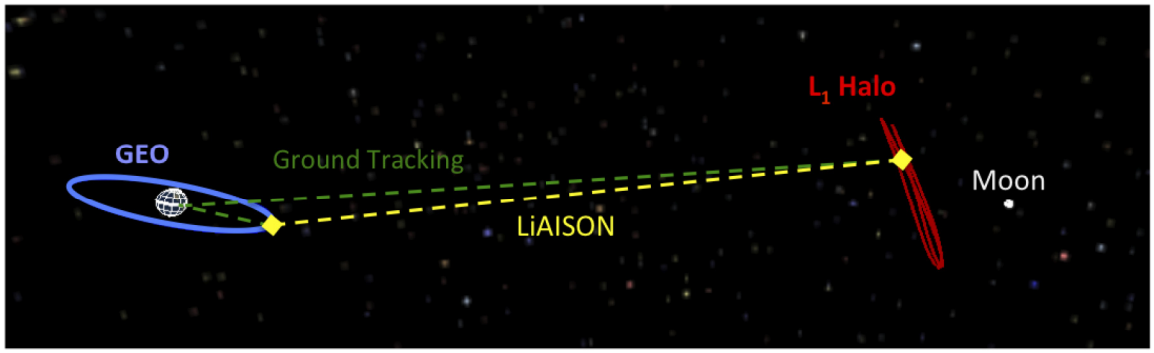

Figure 2. Satellite constellation geometry for truth model simulations for LiAISON and ground tracking viewed in the Earth-Moon rotating frame.

The time evolution of the state dynamics are solved using the TurboProp orbit integration package for orbit propagation.[24] The TurboProp software provides the necessary numerical integration capabilities for the generation of the true trajectories and the filter trajectories. The high-fidelity truth model used in this paper is integrated with a DOPRI8(7)13 integrator with variable step size control.[25] A relative tolerance of 10^{-14} was used with an initial step size of 10 seconds.

A. L_1 Truth Model

The equations of motion for the L_1 truth model have been integrated in the GCRF coordinate system. The L_1 satellite does not use a spherical harmonic model for its representation of Earth's gravitational potential, rather, Earth is assumed to be a point mass. This is considered to be a reasonable estimation since the L_1 orbit is at least 300,000 km from Earth. Third body perturbations are also added to the equations of motion with all of the planets being used as well as the Moon whose states are given by the JPL DE405 ephemeris.[21] A simplified model for SRP given in Eq. 4 is used with an area-to-mass ratio of 0.01 m^2/kg and a coefficient of reflectivity, C_R, of 1.0. Table 2 gives all of the standard LiAISON simulation models used in this analysis with appropriate references.

The halo reference orbit has been generated using a two-step process. First, a set of states has been generated using an analytical expansion described by Richardson and Cary.[26] The reference epoch for the first state in the series has been set to January 1, 2020 ET (Ephemeris Time), the z-axis amplitude, A_z, has been set to 35,500 km, and the initial phase angle of the orbit, ϕ, has been set to zero degrees. Table 1 gives the settings used to generate the halo orbits used in this study. The set includes four states per revolution of the approximate halo orbit and four revolutions about L_1. Ref. 27 describes the benefits gained by adding additional buffer states to this set; hence, an additional revolution of L_1 with four corresponding states is appended to both ends of the set, increasing the number of states in the series to 24.

This set of states is then differentially corrected into the high-fidelity dynamical model previously described with third body perturbations given by the JPL DE405 ephemeris using a multiple shooting differential corrector.[28,29] The differential corrector adjusts the position and velocity of each state, such that the integrated trajectory from one state to the next results in position and velocity discontinuities no greater than 10^{-6} km and 10^{-9} km/s, respectively. These discontinuities are far below the level of error typically

Table 1. L_1 quasi-halo orbit parameters.

Parameter	Value	Comments
A_z	35,500 km	The z-axis amplitude
ϕ	0°	The initial phase angle of the orbit
t_{ref}	1/1/2020 00:00:00 ET	The reference epoch, ephemeris time

observed in the navigation of halo orbiters; hence the resulting trajectory is operationally ballistic.[17] Once converged, the first and last revolution about L_1 are then pruned off, as described by Ref. 27, leaving four continuous revolutions about L_1.

B. GEO Truth Model

The GEO satellite used in this study is placed over the western hemisphere to be visible from U.S. ground stations. The initial latitude and longitude of the GEO satellite is 0.10963 deg N and 80.26889 deg W respectively. GEO truth model equations of motion have also been integrated in the GCRF coordinate system. A 20×20 spherical harmonic gravity field representation of Earth given by GRACE Gravity Model 02 (GGM02C) is used.[30] Third body perturbations are also added to the equations of motion with all of the planets being used as well as the Moon whose states are given by the JPL DE405 ephemeris.[21] A simplified model for SRP given in Eq. 4 is used with an area-to-mass ratio of 0.01 m^2/kg and a coefficient of reflectivity, C_R, of 1.0. Table 2 gives all of the standard LiAISON simulation models used in this analysis with appropriate references.

C. Measurement Generation

LiAISON SST measurements are taken between the GEO satellite and the L_1 satellite during a 9 day period. Both geometric range and range-rate are taken between the two satellites as described in Eq. 18 and Eq. 19. These measurements are corrupted by zero mean Gaussian white noise with a standard deviation of 1 m and 1 mm/s respectively. Fictitious DSN range and range-rate measurements are also taken during this time frame and corrupted by a zero mean Gaussian white noise with a standard deviation of 100 m and 0.1 mm/s respectively. Figure 3 shows the time history of these measurements.

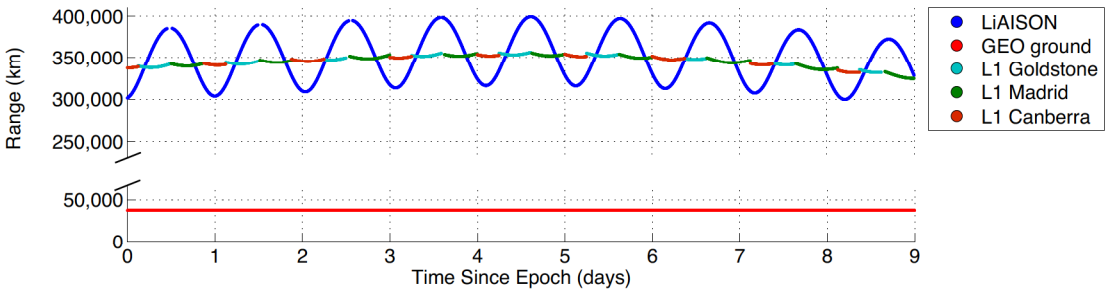

Figure 3. Range observations to the GEO and L_1 orbiter from LiAISON and ground station measurements.

Table 2. Summary of models used in the LiAISON simulations.

Model	LiAISON Standard			Reference
	Reference Frame			
Conventional inertial system	GCRF			–
Precession	1976 IAU			–
Nutation	1980 IAU			–
Planetary ephemerides	JPL DE405			Ref. 21, 22
Polar motion	IERS			–
UT1-TAI	IERS			–
JED/TDB/TT	IERS			–
Station coordinates	Lat. (deg)	Lon. (deg)	Alt. (km)	–
Goldstone	35.247	243.205	1.0711	–
Madrid	40.427	4.251	0.834	–
Canberra	-35.398	148.982	0.692	–
Sky Valley	33.930	243.610	0.445	–
Reference ellipsoid	$a_e = 6378136.3$ m			–
	$1/f = 298.257$			–
	Force Models			
GM	398600.4415 km^3/s^2			Ref. 30
Geopotential	GGM02C & 3–sigma clone 20×20			Ref. 30
N body	JPL DE405			Ref. 21, 22
Solar radiation	solar constant $= 4.5298 \times 10^{-6} Pa$ at 1 AU, conical shadow for Earth.			–
	Measurement Models			
Range	Instantaneous			Eq. 18
Doppler	Instantaneous			Eq. 19

VII. Navigation Simulation Results

The utilization of a truth model simulation allows one to be able to evaluate filter performance under a set of ideal conditions. Since the truth states are known it is easy to investigate filter performance based on initial state perturbations. In order to properly assess filter performance in a real world situation, the filter equations of motion are reduced when compared to the truth model simulations. In this section, the proposed filter is tuned in order to obtain reasonable estimates and uncertainties of the state vector given in Eq. 1. A trade study of the necessary amount of LiAISON and ground observations is also executed. In addition, an analysis of observation scheduling offset is conducted to determine the benefits of having LiAISON and ground observations at different times.

Table 3. Orbit determination filter uncertainties.

Estimation Parameters	*a priori* uncertainty (1-sigma)	Number of Parameters
Spacecraft position	1,000 m	6
Spacecraft velocity	1 mm/s	6
SRP Coefficient	20%	2
Empirical Accelerations		6
Radial	5e-10 m/s^2	–
Transverse	1e-12 m/s^2	–
Normal	1e-12 m/s^2	–
SST range bias	3 m	1
DSN range bias	6 m	3
GEO-supporting ground station range bias	6 m	1
SST measurements		
range	1 m	–
range-rate	1 mm/s	–
DSN measurements		
range	100 m	–
range-rate	0.1 mm/s	–
GEO-supporting ground station measurements		
range	100 m	–
range-rate	1 mm/s	–

A. Filter Dynamical Model and Tuning

The reference trajectory used in the filter contains dynamical errors when compared to the truth model. The filter dynamics use the same dynamical equations previously introduced, however, some of the parameters have been changed to introduce modeling errors. The equations of motion for the GEO satellite in the filter dynamical model consist of a 3-sigma clone of the GGM02C gravity model. Third body perturbations for both satellites are reduced to only the Sun and Moon in addition to the Earth central body force. Both satellites are perturbed by SRP, however, the coefficient of reflectivity is initially in error. It is assumed that the ground station locations are known nearly perfectly and are not estimated or perturbed.

Several filter runs were initially executed for a case in which there were constant observations through LiAISON and ground stations in order to determine the necessary parameters and uncertainties to obtain a position solution that was the most accurate as possible. The estimated parameters and *a priori* uncertainties for the filter runs are given in Table 3. These values are used consistently throughout the analysis done in this paper for each simulation and filter run that is executed. Initial random perturbations of the states within their 3-sigma uncertainties were used during the filter tuning process. For each of these filter executions, consistency and performance of the filter were checked in order to determine if the filter was performing correctly. The total time since epoch that a filter run is executed is 9 days. For each filter run, a comparison to the truth model simulation is used to compare the filter state estimates to the truth states to determine if the estimates are reasonable and within the uncertainty bounds.

B. Trade Study

In this section we investigate the proposed satellite configuration and filter's ability to estimate the parameters listed in Table 3. Over 5000 filter runs were executed to determine the accuracy of certain observation schedules for the LiAISON satellite configuration being investigated. For each simulation there is a minimum of 3 hours of continuous observations every 100 seconds from either the ground station or a LiAISON link between the two satellites. After the 3 hours of continuous observations, an observation gap of "X" hours exists. Observation gaps range from 0 hours (continuous observations) to 72 hours (i.e., very sparse data). Both LiAISON and ground station tracking gaps are varied from continuous tracking to very sparse with a

resolution of 1 hour to create a mesh of possible tracking schedules. The tracking schedules always start with both LiAISON and ground station tracking to begin simultaneously at epoch. The diagonal of the produced mesh will always have LiAISON and ground station tracking for each of the satellites at the exact same time. The tracking schedules are described by the convention (LiAISON Tracking Gap, Ground Tracking Gap). For instance, the schedule (0,0) is continuous LiAISON tracking and ground tracking of both the L_1 and GEO satellites. A tracking schedule of (28,49) has 3 hours of constant tracking to begin with for both LiAISON and ground tracking, followed by a 28 hour gap for LiAISON and a 49 hour gap for ground tracking.

Each of these observation schedules was then used in the processing of tracking data through the Kalman filter previously defined. Figure 4 shows a mesh of the resulting accuracies and uncertainties obtained by the filter runs. Figures 4(a) and 4(b) show the position accuracies determined from the filter runs when compared to the truth model for the L_1 halo and GEO satellite respectively. Figures 4(c) and 4(d) show the position uncertainties estimated from the filter runs for the L_1 halo and GEO satellite respectively. All of the values that are given in the position accuracy and uncertainty meshes are calculated by computing the RMS of the data between the 6^{th} and 9^{th} day past the epoch. The values given in the mesh are determined from the 3D-RMS of the position accuracy when compared to the truth model simulations and 3D-RMS for

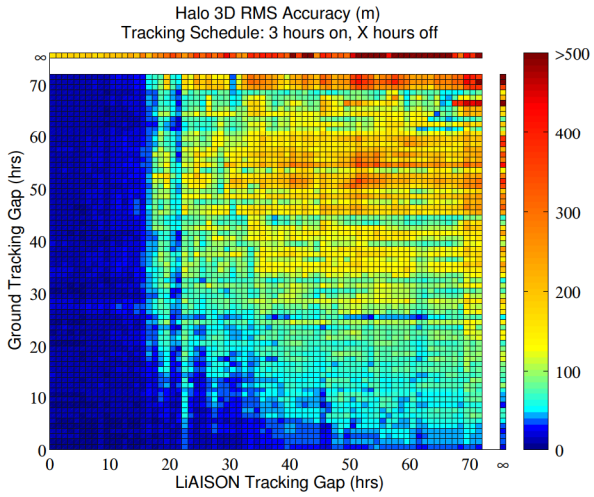

(a) Halo Position Accuracy

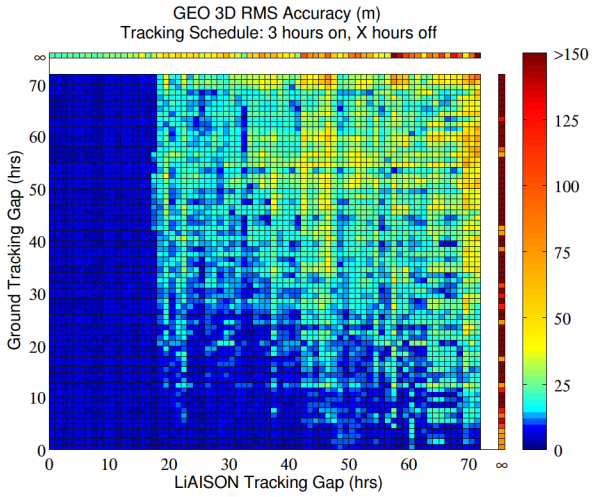

(b) GEO Position Accuracy

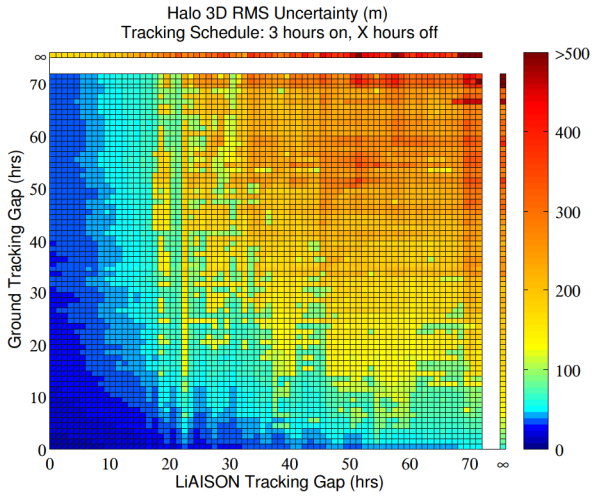

(c) Halo Position 3-sigma Uncertainty

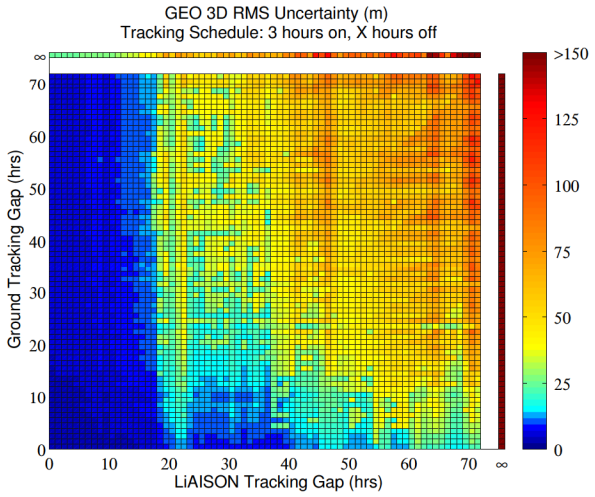

(d) GEO Position 3-sigma Uncertainty

Figure 4. Orbit determination accuracy and 3-sigma uncertainty for various amounts of LiAISON and ground station tracking.

the position uncertainties given from the filter runs. The uncertainty values given in the mesh are 3-sigma values. Values over an accuracy or uncertainty of 500 meters for the halo orbiter and 150 meters for the GEO orbiter are represented by the same color. The far column and row denoted by an observation tracking gap of ∞ corresponds to only LiAISON or ground station tracking data. This is provided as a check to see how accurate one tracking method is completely separate from the other. Tracking of the halo orbiter with continuous ground tracking is the most accurate with an uncertainty of about 70 meters. Continuous ground tracking of the GEO satellite using only radiometric data from one ground station does not reduce the *a priori* uncertainty. Continuous LiAISON only tracking provides reasonable estimates for both the halo and GEO orbiters with an uncertainty of about 160 meters and 24 meters respectively.

Relatively continuous LiAISON tracking (continuous to 20 hour gaps) is roughly equivalent to the uncertainty obtained from a ground tracking schedule of continuous tracking to 10 hour gaps. In order to achieve a position uncertainty of less than 200 m for the halo orbiter, a ground track every day is necessary. To achieve the same accuracy for the halo orbiter using only LiAISON tracking, a tracking schedule with 3 hours on continuous tracking followed by a 12 hour gap is enough. This tracking schedule results in the uncertainty of the GEO satellite position being about 30 meters. The addition of a three hour pass of ground tracking every 3 days to a LiAISON tracking scheme on a 12 hour gap schedule reduces the uncertainty of the halo orbit to about 50 meters and the GEO orbit to about 10 meters. While continuous LiAISON measurements can obtain reasonable position accuracies for both satellites, the addition of relatively few ground tracking passes can greatly improve the solution.

Ideally, one would like to have as few tracking passes from LiAISON and ground tracking as possible to obtain an accurate solution. There exists an area of this analysis from which relatively accurate estimates can be obtained using very few tracking passes. The tracking schedules for this region are 28-30 hour gaps for LiAISON and 48-56 hour gaps for ground tracking. In this region the halo orbiter's uncertainty is around 110 meters while the GEO accuracy is about 35 meters. With very few measurements from both LiAISON and ground tracking, reasonable estimates of both satellites states are obtained.

Figure 5 shows the time history of the position uncertainty for various tracking schedules for a few interesting cases that arise from the trade study analysis. The tracking schedules shown are continuous tracking (0,0), continuous LiAISON and sparse ground tracking (0,72), sparse LiAISON and continuous ground tracking (72,0), and a point from the previously described sparse tracking region that gives reasonable estimates (28,49).

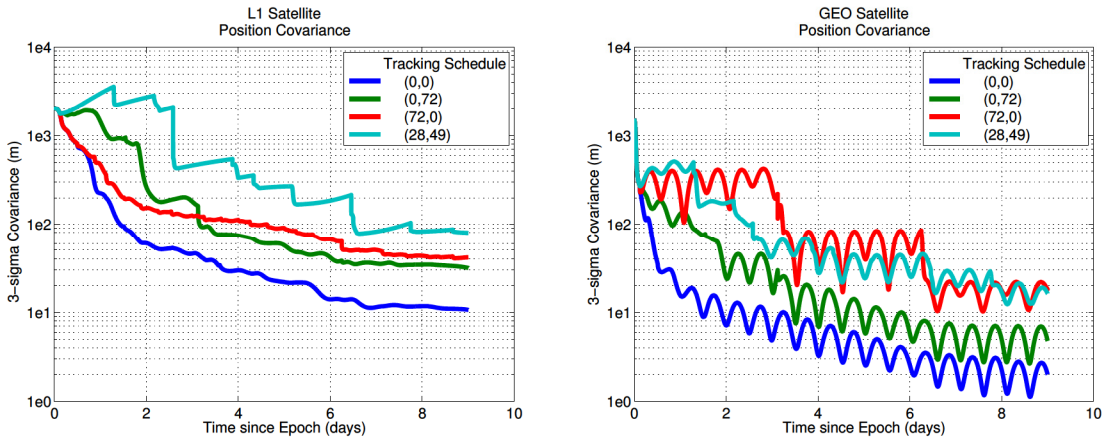

(a) Halo (b) GEO

Figure 5. Time history comparison of 3-sigma position uncertainty for various tracking schedules.

The position covariances shown in Figure 5 give the filtered updated covariance and filter predicted covariance to make the comparison continuous for all cases. As one would expect, the continuous tracking schedule of (0,0) gives the best results. Here both LiAISON and ground tracking are combined for continuous observation of the two satellites. Final position uncertainties are on the order of 10 meters for the L_1 orbiter and 3 meters for the GEO satellite.

The next most accurate estimates come from the tracking schedules of (0,72) and (72,0). Both of these tracking schedules produce roughly the same uncertainty for the halo orbiter. Initially, (72,0) has less

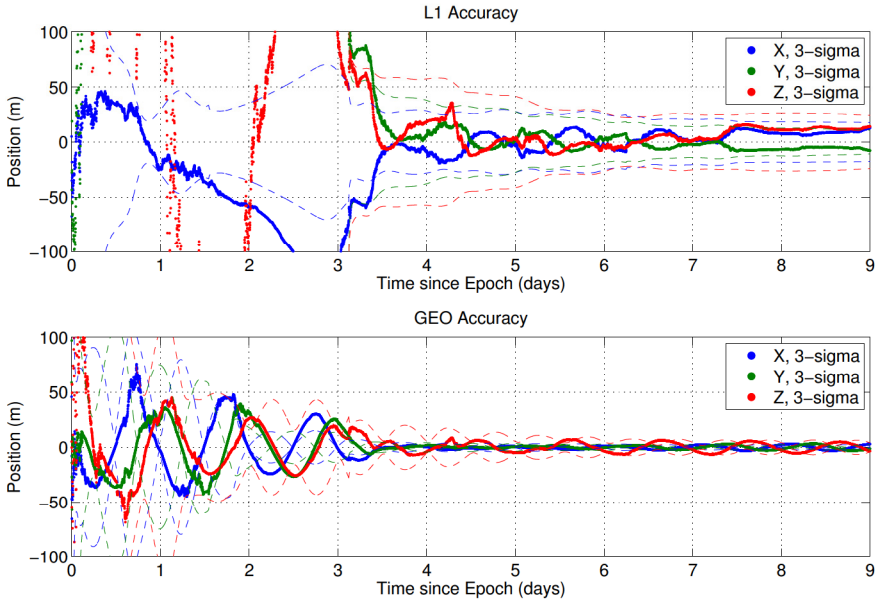

Figure 6. Position accuracy and uncertainty for LiAISON constellation for a tracking schedule with continuous LiAISON tracking and 3 hours of ground tracking followed by 72 hour observation gap (0,72).

uncertainty than (0,72), but the second tracking pass from the DSN around 3 days helps lower the uncertainty to less than (72,0). After this second DSN pass, the tracking schedule (0,72) always has less uncertainty than (72,0) but the difference is only 10's of meters. There is a large difference in the uncertainty, however, for the GEO satellite. The tracking schedule (0,72) for the GEO satellite is the most accurate showing that the LiAISON data type defined in this analysis is better suited for estimating the state of the GEO satellite than the radiometric only data from one tracking station. One can notice a large decrease in the uncertainty for the (72,0) case when a LiAISON measurement pass is obtained around day 3. If this LiAISON pass did not exist, the uncertainty in the GEO satellite's position would stay around 500 m instead of reducing to 100 m. The next LiAISON pass for this case occurs at about 6 days, and again, the uncertainty in the GEO satellite

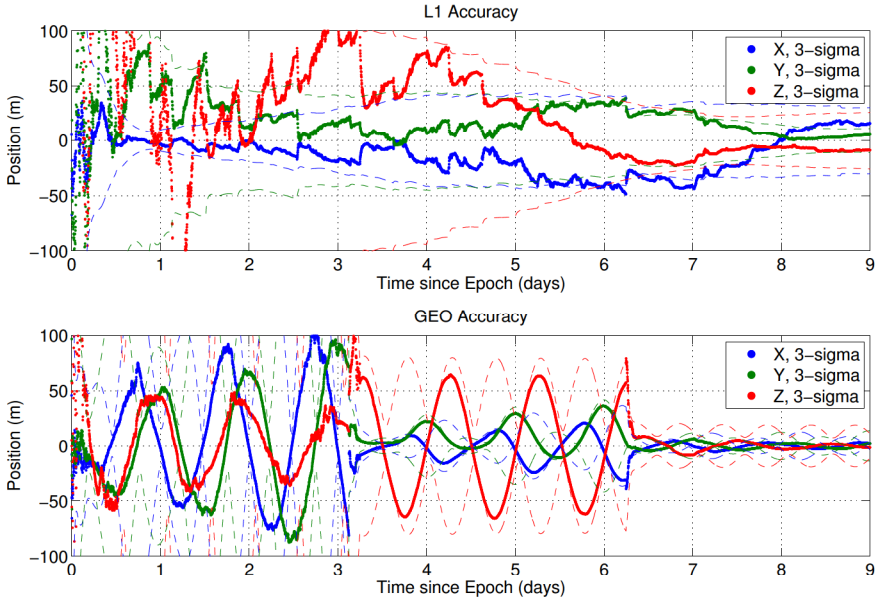

Figure 7. Position accuracy and uncertainty for LiAISON constellation for a tracking schedule with 3 hours of LiAISON followed by 72 hour observation gap and continuous ground tracking (72,0).

is reduced significantly. Figures 6 and 7 show the position accuracy and 3-sigma uncertainties for a tracking schedule of (0,72) and (72,0). After 3 days of observation processing, the accuracy and uncertainty of the L_1 satellite for both tracking schedules is less than 100 m. The GEO satellite's accuracy and uncertainty for the (0,72) schedule is significantly less than the (72,0) schedule. The (0,72) GEO uncertainty is less than 100 m after 1 day of observation processing while it takes 3 days for the (72,0) schedule. The uncertainty reduction due to the LiAISON measurement updates at 3 and 6 days is clearly visible in Figure 7.

The final schedule given in Figure 5 is (28,49). The tracking schedule of (28,49) falls within a region of the trade study where 28-30 hour gaps for LiAISON and 48-56 hour gaps for ground tracking produces an uncertainty of about 110 m and 35 m the halo and GEO satellite after 9 days of tracking. This tracking schedule of (28,49) obtains position uncertainties of less than 100 m and 30 m for the halo and GEO satellites respectively after 9 days of tracking. While the uncertainty is higher for the halo orbiter when compared to the other tracking schedules, the uncertainty of the GEO satellite is comparable to constant ground tracking with sparse LiAISON measurements, (72,0). Figure 8 shows the time history of the position accuracy and 3-sigma uncertainty for the tracking schedule of (28,49). The reduction in uncertainty for the L_1 satellite due to measurement updates can clearly be seen. The uncertainty of the L_1 satellite is well above 1 km for the first 2 days and does not reduce to under 100 m until 6 days of observations. The GEO satellite uncertainty is less than 100 m after 2 days of observation processing and reduces down to 30 m after 6 days.

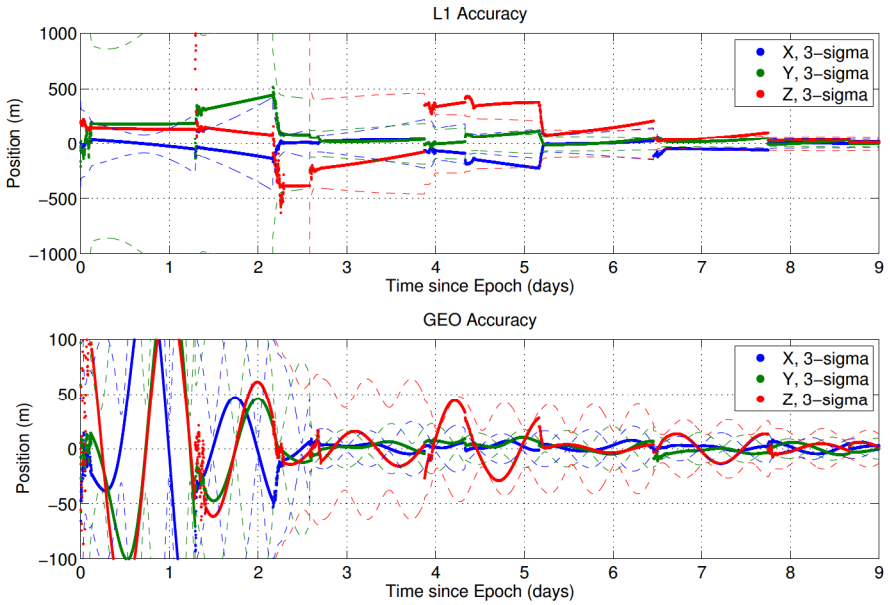

Figure 8. Position accuracy and uncertainty for LiAISON constellation for a tracking schedule with 3 hours of LiAISON followed by 28 hour observation gap and 3 hours of ground tracking followed by 49 hour observation gap (28,49).

Another feature that shows up in the trade study analyses is the growth in uncertainty around 22 hours which is a result of a worsening observation geometry. In the trade study analysis, there was a ridge of more inaccurate solutions and uncertainty for tracking schedules that involved a resonance of around 22 hours for both the L_1 and GEO satellites. Another resonance is noticeable at roughly 44 hours for the GEO satellite. These resonances are caused by a periodic condition in which the LiAISON constellation is observing the GEO satellite at roughly the same geometry as the previous day.

C. Scheduling Offset

In the previous analyses, the diagonal of the produced mesh always had LiAISON and ground station tracking for each of the satellites at the exact same time. Measurements occurring at the exact same time from both LiAISON and ground stations affect the performance of the filter in a certain way. In this section, we investigate filter performance for this diagonal by offsetting the times at which the measurements occur. Simulations and filter runs will always have equal amounts of measurements, 3 hours on and "X" hours off, for both LiAISON and ground station tracking. The times at which these measurements are taken will be

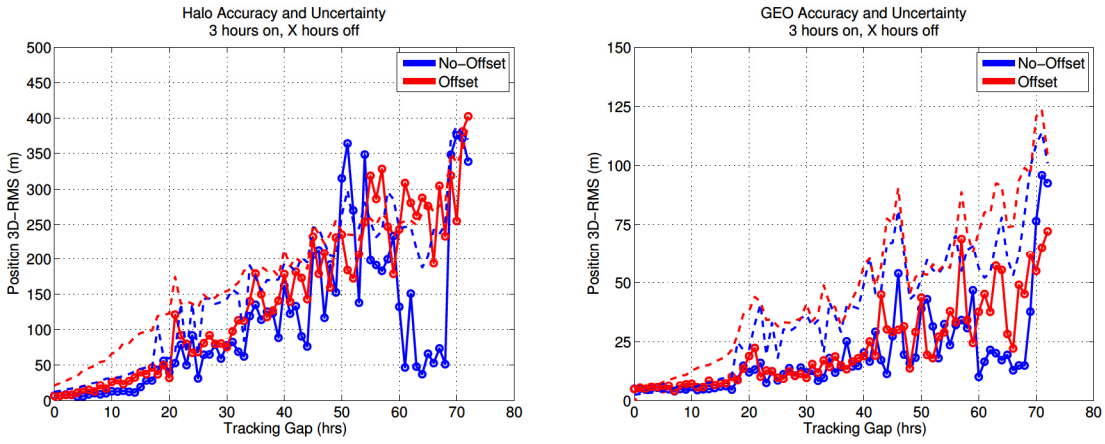

(a) Halo (b) GEO

Figure 9. LiAISON L_1 and GEO measurement offset analysis. Solid lines represent 3D-RMS accuracy and dashed lines represent 3-sigma uncertainty.

offset and compared to when the measurements are taken simultaneously.

The truth simulation used in this study is the same as before with the same dynamical models. The only thing that has changed is the times at which LiAISON observations or ground station measurements are taken of the L_1 and GEO satellites. Observations generated during this analysis always begin with LiAISON measurements taken for the first three hours followed by a gap of no measurements for "X" hours. Ground station observations are calculated to start exactly half way through the LiAISON observation gap. Three hours of continuous ground station measurements spaced at an interval off 100 seconds are calculated. Preference to the main ground station that has the most visibility with an elevation mask of 10 degrees is given as the primary tracker of the satellites. Once the measurements are obtained for that three hour period, the ground station measurements experience a gap of exactly "X" hours (the same gap time as the LiAISON measurements). The process is then repeated to always have ground station measurements to begin at exactly half of the LiAISON observation gap.

Several filter runs were executed to determine the effects of an observation offset for the diagonal elements of the previous trade study mesh. Simulations begin with completely continuous LiAISON and ground station tracking of the L_1 and GEO satellites. An observation gap of 1 hour is then added until there is a gap of 72 hours. Figure 9(a) shows the 3D-RMS position accuracy and uncertainty of the halo orbiter for the offset observation case as well as the no-offset observation case. The GEO satellite's 3D-RMS position accuracy and uncertainty is shown in Figure 9(b) for the offset observation case as well as the no-offset observation case.

A few features show up in the offset analysis for this LiAISON constellation. The results show that neither satellite's uncertainty or accuracy is impacted significantly by the scheduling offset. The filter solution accuracy and uncertainty are relatively the same for both cases. Another feature that shows up in both analyses is the growth in uncertainty around 22 hours which is a result of a worsening observation geometry. In the trade study analysis, there was a ridge of more inaccurate solutions and uncertainty for tracking schedules that involved a resonance of around 22 hours for both the L_1 and GEO satellites. This growth in uncertainty occurs in the offset analysis as well. Another resonance in noticeable at roughly 44 hours for the GEO satellite.

VIII. Conclusion

A new LiAISON constellation configuration involving two satellites, one in orbit about the Earth-Moon L_1 and one in geosynchronous Earth orbit, has been analyzed. This study demonstrates that the relative and absolute navigation of two satellites at GEO and L_1 is possible through the use of satellite-to-satellite range and range-rate measurements. In addition, this measurement type can supplement and significantly improve radiometric measurements taken from the Deep Space Network for satellite navigation.

A complete study of observation scheduling was done for the GEO and L_1 LiAISON constellation. Filter accuracies and uncertainties obtained through high-fidelity simulations match that of current NASA practices for the Artemis mission. The supplement of LiAISON observations to ground tracking passes can significantly reduce the uncertainty of an orbit determination solution. Several cases have been analyzed and compared. Among these were continuous ground and LiAISON tracking, continuous ground and sparse LiAISON tracking, continuous LiAISON and sparse ground tracking, and relatively sparse tracking for both LiAISON and ground. While continuous tracking of both data types produced the best results, continuous LiAISON with sparse ground tracking produced nearly the same accuracies as continuous ground with sparse LiAISON tracking. This shows that the inclusion of a necessary amount of LiAISON tracking can significantly reduce the number of ground tracks necessary to obtain a given accuracy, which can significantly reduce the costs of ground tracking. It was also shown that there exists a region in which viable tracking schedules with relatively sparse data can produce position accuracies of about 100 m for the halo orbiter and less than 30 m for the GEO satellite. These types of tracking schedules would allow for a reduction in DSN time with very minimal interaction with the LiAISON constellation while maintaining a given position uncertainty.

A simple study was also conducted to determine if the effect of obtaining observations at the same epoch impacted the solution accuracy and uncertainty. In this study, a tracking schedule that contained the same observation gaps was adjusted to allow for observations to come in at different times but maintain the observation gap duration. There was no significant impact on the accuracy and uncertainty by acquiring observations at different times. During this analysis, interesting features were enhanced for which poor observation geometry on a schedule of roughly 22 hours was experienced. During this timeframe, the geometry of the LiAISON and GEO configuration is such that every observation time the GEO satellite is being sampled in roughly the same position and geometry as it was the previous time. This reduces the necessary information in order to obtain a more accurate solution. It is suggested through this study that one try to minimize the times in which one takes measurements during this period.

The configuration and simulations studied in this paper are representative of a realistic LiAISON navigation configuration. The analysis has been done in a high-fidelity regime with the necessary dynamical errors that plague the orbital regime. These dynamical errors were overcome to obtain accurate navigation solutions using only radiometric data from a satellite based at the Earth-Moon libration point L_1. It has been shown that absolute navigation is possible for a GEO satellite and a lunar libration orbiter using minimal ground tracks that have been supplemented with LiAISON observation data. This study has demonstrated LiAISON's potential capability as an addition to the Deep Space Network to help improve navigation solutions for future missions.

Acknowledgments

The authors would like to thank the JPL Center Innovation Fund (CIF) Program, sponsored by NASA Office of the Chief Technologist (OCT), which has supported this research.

The research presented in this paper has been partially carried out at the Jet Propulsion Laboratory, California Institute of Technology, under a contract with the National Aeronautics and Space Administration.

References

[1]Hill, K., Lo, M. W., and Born, G. H., "Linked, Autonomous, Interplanetary Satellite Orbit Navigation (LiAISON)," *AAS/AIAA Astrodynamics Specialist Conference*, No. AAS 05-399, AAS/AIAA, Lake Tahoe, CA, August 7–11, 2005.

[2]Hill, K., Born, G. H., and Lo, M. W., "Linked, Autonomous, Interplanetary Satellite Orbit Navigation (LiAISON) in Lunar Halo Orbits," *AAS/AIAA Astrodynamics Specialist Conference*, No. AAS 05-400, AAS/AIAA, Lake Tahoe, CA, August 7–11, 2005.

[3]Hill, K., Parker, J. S., Born, G. H., and Demandante, N., "A Lunar L2 Navigation, Communication, and Gravity Mission," *AIAA/AAS Astrodynamics Specialist Conference*, No. AIAA 2006-6662, AIAA/AAS, Keystone, Colorado, August 2006.

[4]Hill, K., Lo, M. W., and Born, G. H., "Liaison Navigation in the Sun-Earth-Moon Four-Body Problem," *AAS/AIAA Spaceflight Dynamics Conference*, No. AAS 06-221, AAS/AIAA, Tampa, FL, January 22–26, 2006.

[5]Hill, K. and Born, G. H., "Autonomous Interplanetary Orbit Determination Using Satellite-to-Satellite Tracking," *AIAA Journal of Guidance, Control, and Dynamics*, Vol. 30, No. 3, May–June 2007.

[6]Hill, K., *Autonomous Navigation in Libration Point Orbits*, Ph.D. thesis, University of Colorado, Boulder, Colorado, 2007.

[7]Villac, B., Chow, C., Lo, M., Hintz, G., and Nazari, Z., "Dynamic Optimization of Multi-Spacecraft Relative Navigation Configurations in the Earth-Moon System," *George H. Born Symposium*, AAS, Boulder, Colorado, 13–14 May 2010.

[8]Hamera, K., Mosher, T., Gefreh, M., Paul, R., Slavkin, L., and Trojan, J., "An Evolvable Lunar Communication and Navigation Constellation Concept," *IEEE Aerospace Conference*, No. IEEE 1491, IEEE, Big Sky, Montana, 28 April–1 May 2008.

[9]Tombasco, J., *Orbit Estimation of Geosynchronous Objects via Ground-Based and Space-Based Optical Tracking*, Ph.D. thesis, University of Colorado, Boulder, Colorado, 2011.

[10]Parker, J. S., Anderson, R. L., Born, G. H., Fujimoto, K., Leonard, J. M., and McGranaghan, R. M., "Navigation between geosynchronous and lunar L1 orbiters," *Submitted to AAS/AIAA Astrodynamics Specialist Conference*, AAS/AIAA, Minneapolis, MN, August 13–16, 2012.

[11]Fujimoto, K., Leonard, J. M., McGranaghan, R. M., Parker, J. S., Anderson, R. L., and Born, G. H., "Simulating the LiAISON Navigation Concept in a GEO + Earth-Moon Halo Constellation," *Accepted to 23rd International Symposium on Space Flight Dynamics*, Pasadena, California, October 29 – November 2 2012.

[12]Wallace, S., Sabol, C., and Carter, S., "Optical Sensor Calibration using GPS Reference Orbits," *MIT/Lincoln Lab Space Control Workshop*, Lexington, MA, March 1997.

[13]Sabol, C. A., *A role for Improved Angular Observations in Geosynchronous Orbit Determination*, Ph.D. thesis, University of Colorado, Boulder, Colorado, 1998.

[14]Moreau, M. C., Axelrad, P., Garrison, J. L., and Long, A., "GPS Receiver Architecture and Expected Performance for Autonomous Navigation in High Earth Orbits," *Navigation*, Vol. 47, No. 3, 2000, pp. 191–204.

[15]Broschart, S. B., Chung, M. J., Hatch, S. J., Ma, J. H., Sweetser, T. H., Weinstein-Weiss, S. S., and Angelopoulos, V., "Preliminary Trajectory Design for the ARTEMIS Lunar Mission," *Proceedings of the AAS/AIAA Astrodynamics Specialist Conference held 9-13 August 2009, Pittsburgh, Pennsylvania*, edited by A. V. Rao, T. A. Lovell, F. K. Chan, and L. A. Cangahuala, Vol. 134 of *Advances in Astronautical Sciences*, AAS/AIAA, Univelt Inc., San Diego, CA, 2009.

[16]Woodard, M., Folta, D., and Woodfork, D., "ARTEMIS: The First Mission to the Lunar Libration Orbits," *21st International Symposium on Space Flight Dynamics*, Centre National d'Études Spatiales, Toulouse, France, September 28 – October 2, 2009.

[17]Folta, D., Woodard, M., and Cosgrove, D., "Stationkeeping of the First Earth-Moon Libration Orbiters: The ARTEMIS Mission," *Proceedings of the 2011 AAS/AIAA Astrodynamics Specialists Conference*, 2011.

[18]Woodard, M., Cosgrove, D., Morinelli, P., Marchese, J., Owens, B., and Folta, D., "Orbit Determination Of Spacecraft In Earth-Moon L1 And L2 Libration Point Orbits," *Proceedings of the 2011 AAS/AIAA Astrodynamics Specialists Conference*, AAS 11–514, July 31 – August 4, 2011, Girdwood, Alaska 2011.

[19]Gottlieb, R. G., "Fast Gravity, Gravity Partials, Normalized Gravity, Gravity Gradient Torque and Magnetic Field: Derivation, Code and Data," *Tech. Rep. NASA Contractor Report 188243*, 1993.

[20]Montenbruck, O. and Gill, E., *Satellite Orbits: Models, Methods and Applications*, Springer-Verlag, Netherlands, corrected 3rd printing 2005 ed., 2000.

[21]Standish, E. M., "JPL planetary and lunar ephemerides, DE405/LE405," *Jet Propulsion Laboratory Interoffice Memorandum IOM 312F-98-048*, Aug. 26 1998.

[22]Hoffman, D., *A Set of C Utility Programs for Processing JPL Ephemeris Data*, Johnson Space Center, 1998.

[23]Tapley, B., Schutz, B., and Born, G., *Statistical Orbit Determination*, Academic Press, 2004.

[24]Hill, K. and Jones, B. A., *TurboProp Version 4.0*, Colorado Center for Astrodynamics Research, May 2009.

[25]Prince, P. J. and Dormand, J. R., "High Order Embedded Runge-Kutta Formulae," *Journal of Computational and Applied Mathematics*, Vol. 7, 1981, pp. 67–75.

[26]Richardson, D. L. and Cary, N. D., "A Uniformly Valid Solution for Motion of the Interior Libration Point for the Perturbed Elliptic-Restricted Problem," *AAS/AIAA Astrodynamics Specialist Conference*, No. AAS 75-021, AAS/AIAA, July 1975.

[27]Parker, J. S., *Low-Energy Ballistic Lunar Transfers*, Ph.D. thesis, University of Colorado, Boulder, Colorado, 2007.

[28]Pernicka, H. J., *The Numerical Determination of Lissajous Orbits in the Circular Restricted Three-Body Problem*, Master's thesis, Purdue University, December 1986.

[29]Wilson, R., "Derivation of Differential Correctors Used in GENESIS Mission Design," Tech. Rep. JPL IOM 312.I-03-002, Jet Propulsion Laboratory, California Institute of Technology, 2003.

[30]Tapley, B., Ries, J., Bettadpur, S., Chambers, D., Cheng, M., Condi, F., Gunter, B., Kang, Z., Nagel, P., Pastor, R., Pekker, T., Poole, S., and Wang, F., "GGM02 - An Improved Earth Gravity Field Model from GRACE," *Journal of Geodesy*, Vol. 79, No. 8, 2005, pp. 467–478.